



ELSEVIER

Contents lists available at ScienceDirect

## Physics of the Earth and Planetary Interiors

journal homepage: [www.elsevier.com/locate/pepi](http://www.elsevier.com/locate/pepi)Thermoelastic properties of MgSiO<sub>3</sub>-majorite at high temperatures and pressures: A first principles studyYancheng Lou<sup>a,b,c,d</sup>, Stephen Stackhouse<sup>d</sup>, Andrew M. Walker<sup>d</sup>, Zhigang Zhang<sup>a,b,c,\*</sup><sup>a</sup> Key Laboratory of Earth and Planetary Physics, Institute of Geology and Geophysics, Chinese Academy of Sciences, Beijing 100029, China<sup>b</sup> College of Earth and Planetary Sciences, University of Chinese Academy of Sciences, Beijing 100049, China<sup>c</sup> Innovation Academy for Earth Science, Chinese Academy of Sciences, Beijing 100029, China<sup>d</sup> School of Earth and Environment, University of Leeds, Leeds LS2 9JT, UK

## ARTICLE INFO

## Keywords:

Majorite

Garnet

Elastic properties

Anisotropy

Transition zone

First principles

## ABSTRACT

As the major component of garnet, the second most abundant phase in Earth's transition zone, MgSiO<sub>3</sub>-majorite plays a fundamental role in controlling the state and dynamics of Earth's mantle. However, due to challenges of experiments and simulations, there are still very limited data on the elastic properties of MgSiO<sub>3</sub>-majorite at simultaneously high temperatures and pressures. In this study, we have carried out extensive first principles calculations to determine the thermoelastic properties of MgSiO<sub>3</sub>-majorite up to 2000 K and 40 GPa. We find that the elastic constants of MgSiO<sub>3</sub>-majorite change significantly over the temperature and pressure range studied, with noticeable non-linearities in their pressure dependences. The seismic anisotropy of MgSiO<sub>3</sub>-majorite is high and generally increases with pressure. It is much higher than that of the other end-members of garnet and ringwoodite, which makes it the most anisotropic mineral in assemblages expected in the lower transition zone. Based on our calculated elastic moduli and with careful elimination of systematic errors, we establish a third-order Birch-Murnaghan-Mie-Grüneisen model for MgSiO<sub>3</sub>-majorite with the parameters:  $V_0 = 114.1 \text{ cm}^3/\text{mol}$ ,  $K_0 = 163.6 \text{ GPa}$ ,  $G_0 = 86.4 \text{ GPa}$ ,  $K_0' = 4.44$ ,  $G_0' = 1.16$ ,  $\gamma_0 = 1.08$ ,  $q_0 = 0.48$ ,  $\eta_{50} = 0.76$ , and  $\theta_0 = 822.5 \text{ K}$ . Integrating our results into a thermodynamic model able to predict the properties of mantle assemblages, we find that a pyrolite composition produces velocities that agree with the seismic model AK135 in the upper transition zone. In the lower transition zone, a pyrolite composition fits well with some specific local observations, but a mechanical mixture with 18% basalt and 82% harzburgite is in better agreement with the global seismic model PREM. The much larger abundance of MgSiO<sub>3</sub>-majorite in the garnet phase of harzburgite suggests that the anisotropy in the lower transition zone may not be negligible and would be observable at least in the heterogeneous zones near subducting slabs.

## 1. Introduction

From the constraints provided by seismic observations and mineral physics, garnet is recognized to be the major phase in the Earth's upper mantle and transition zone (Stixrude and Lithgow-Bertelloni, 2012). Accounting for up to over 40 mol% in the normal transition zone and over 90 mol% in subducting slabs (Stixrude and Lithgow-Bertelloni, 2012), it largely controls the thermal and chemical evolution of these areas. To strive for a better understanding of the role played by garnet, it is important to know its thermoelastic properties over a wide range of temperatures and pressures, which are mainly determined by those of its constituent components i.e. pyrope, almandite, grossular, majorite, etc.

As a major end-member of garnet, MgSiO<sub>3</sub>-majorite becomes increasingly important from the base of the upper mantle and is present throughout the transition zone (Ringwood, 1967). However, due to challenges in measuring elastic properties at simultaneously high temperature and pressure, most experimental studies of MgSiO<sub>3</sub>-majorite only report values at ambient conditions (Angel et al., 1989; Bass and Kanzaki, 1990; Gwanmesia et al., 1998; Heinemann et al., 1997; Kato and Kumazawa, 1985; Kavner et al., 2000; Liu et al., 2019; Matsubara et al., 1990; Pacalo and Weidner, 1997; Sawamoto, 1987; Sinogeikin and Bass, 2002a; Sinogeikin et al., 1997). Only limited data have been reported at high-pressure and room temperature (Hazen et al., 1994; Yagi et al., 1992). In addition, there are only a small number of simulation studies reporting the elastic properties of MgSiO<sub>3</sub>-

\* Corresponding author at: Key Laboratory of Earth and Planetary Physics, Institute of Geology and Geophysics, Chinese Academy of Sciences, Beijing 100029, China.

E-mail address: [zgzhang@mail.iggcas.ac.cn](mailto:zgzhang@mail.iggcas.ac.cn) (Z. Zhang).

<https://doi.org/10.1016/j.pepi.2020.106491>

Received 2 December 2019; Received in revised form 27 March 2020; Accepted 8 April 2020

Available online 19 April 2020

0031-9201/© 2020 The Authors. Published by Elsevier B.V. This is an open access article under the CC BY license

(<http://creativecommons.org/licenses/by/4.0/>).

majorite, due to the significant computational expense associated with modeling the relatively large unit cell. Most studies only report values at static conditions (De La Pierre and Belmonte, 2016; Hernandez et al., 2015; Li et al., 2007; Pigott et al., 2015; Vinograd et al., 2006; Yu et al., 2011). One study reports data for the bulk modulus of MgSiO<sub>3</sub>-majorite at simultaneous high temperature and pressure but provides no values for the shear modulus or elastic constants (Yu et al., 2011). There are even fewer studies that report values for seismic anisotropy (Li et al., 2007; Pacalo and Weidner, 1997; Pigott et al., 2015).

In this study we have performed first principles calculations to determine the thermoelastic properties of MgSiO<sub>3</sub>-majorite over a wide range of temperatures and pressures. We determine elastic constants, anisotropies, bulk and shear moduli, seismic velocities and other thermodynamic properties. After carefully eliminating systematic errors in the simulation results, we obtain a third-order Birch-Murnaghan-Mie-Grüneisen model for MgSiO<sub>3</sub>-majorite. Using this model to predict the properties of mineral assemblages in the transition zone, we find that a mechanical mixture of basalt and harzburgite may be a better interpretation than the equilibrium pyrolytic model for global seismic observations in the lower transition zone.

## 2. Computational details

### 2.1. Crystal structure

MgSiO<sub>3</sub>-majorite, Mg<sub>3</sub>(Mg,Si)[SiO<sub>4</sub>]<sub>3</sub>, is a garnet-structured mineral with tetragonal space group *I*<sub>4</sub><sub>1</sub>/*a*. The crystal structure of MgSiO<sub>3</sub>-majorite includes three different types of polyhedra: tetrahedra, octahedra, and dodecahedra. Tetrahedral sites are occupied by Si<sup>4+</sup>, octahedral sites are occupied by Mg<sup>2+</sup> and Si<sup>4+</sup> and dodecahedral sites are occupied by Mg<sup>2+</sup> (Fig. 1). There are two distinct octahedral sites with Wyckoff positions of 8c and 8d. In the ordered *I*<sub>4</sub><sub>1</sub>/*a* structure, all 8c sites are occupied by Si<sup>4+</sup> cations and all 8d sites by Mg<sup>2+</sup>. At sufficiently high temperatures, a random distribution of Si<sup>4+</sup> and Mg<sup>2+</sup> in these two sites is possible, leading to disordered structures with higher symmetry (Angel et al., 1989; Li et al., 2007).

The starting structure of MgSiO<sub>3</sub>-majorite used in the simulations was the experimentally determined structure (Angel et al., 1989), which has also been used in previous works (Pigott et al., 2015; Vinograd et al., 2006; Yu et al., 2011). It is a tetragonal unit cell with 160 atoms (8 Mg<sub>3</sub>(Mg,Si)[SiO<sub>4</sub>]<sub>3</sub> units). According to the study of Yu et al. (2011), the order-disorder transition between magnesium and silicon in the octahedral sites occurs at about 3600 K and the long-range order parameter, which is 1.0 for a completely ordered state and 0.0 for a completely disordered state, is always larger than 0.97 when the temperature is lower than 2500 K. Therefore, in line with Yu et al. (2011), we used the lowest energy ordered *I*<sub>4</sub><sub>1</sub>/*a* structure (as shown in Fig. 1) throughout this study. Simulations of some other cation-ordering arrangements yield comparable results to those described here, as shown in Table S1.

### 2.2. First principles simulations

We determined the effects of pressure and temperature on the structure and elasticity of majorite using first principles simulations. This approach couples density functional theory (DFT; Hohenberg and Kohn, 1964; Kohn and Sham, 1965), used to evaluate the forces between atoms arising from the electronic structure, with Newtonian mechanics, used to simulate the thermal motion of atoms. Simulations were performed using the Vienna ab initio simulation package (VASP; Kresse and Furthmüller, 1996a, 1996b; Kresse and Hafner, 1993; Kresse and Joubert, 1999), which makes use of a plane-wave expansion of the Kohn-Sham wavefunctions (Payne et al., 1992) and the projector augmented wave (PAW) approach for the description of core electrons (Blöchl, 1994; Kresse and Joubert, 1999). The PBE (Perdew et al., 1996) implementation of GGA (generalized gradient approximation) to the exchange-correlation functional was used throughout. The core radii of the PAW pseudopotentials used were 1.06 Å for Mg (valence configuration with p semi-core valence state is 2p<sup>6</sup>3s<sup>2</sup>), 0.79 Å for Si (3s<sup>2</sup>3p<sup>2</sup>) and 0.80 Å for O (2s<sup>2</sup>2p<sup>4</sup>).

For the static calculations, we used a 2 × 2 × 2 Brillouin zone sampling grid, an energy for the plane-wave cutoff of 800 eV and an

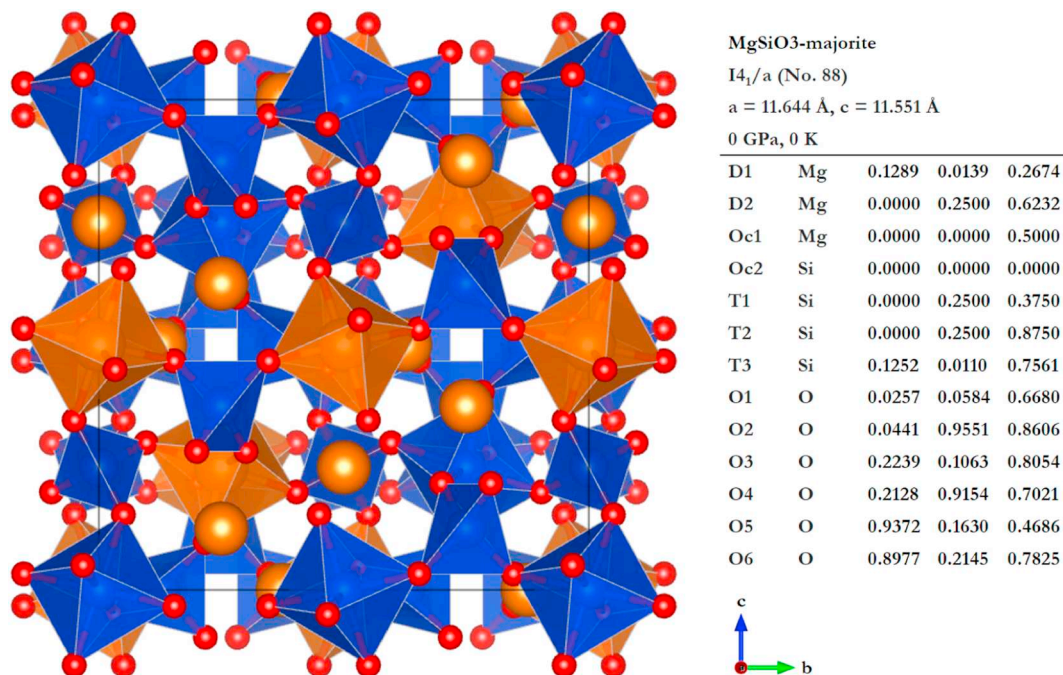


**Fig. 1.** Crystal structure of MgSiO<sub>3</sub>-majorite. Orange spheres represent Mg<sup>2+</sup> which occupy dodecahedral sites (the interstitial site between tetrahedral and octahedral sites). Blue octahedra are occupied by Si<sup>4+</sup> and orange octahedra are occupied by Mg<sup>2+</sup>. Blue tetrahedra are occupied by Si<sup>4+</sup>. Crystallographic data (cell parameters and basis vectors) obtained at 0 K and 0 GPa are also shown. (For interpretation of the references to color in this figure legend, the reader is referred to the web version of this article.)

**Table 1**  
Comparisons of the lattice parameters of MgSiO<sub>3</sub>-majorite.

	a (Å)	c (Å)	c/a	V (Å <sup>3</sup> )
<i>P</i> = 0 GPa				
Experiment, room temperature				
Angel et al. (1989)	11.501(1)	11.480(2)	0.998(2)	1518.6(4)
Liu et al. (2017)	11.509(21)	11.446(43)	0.995	1516.1(60)
Sinogeikin et al. (1997)	11.500(35)	11.445(50)	11.445(50)	1513.6(15)
Pacalo and Weidner (1997)	11.514(1)	11.423(1)	0.992	1514.3
Calculation, static				
This study (PBE-GGA)	11.644	11.551	0.992	1566.0
Li et al. (2007) (PW91-GGA)	11.645	11.554	0.992	1566.7
Pigott et al. (2015) (USPP-PW91-GGA)	11.638	11.528	0.991	1561.3
Vinograd et al. (2006) (DFT-GGA)	11.670	11.561	0.991	1557.5
Hernandez et al. (2015) (PW91-GGA)	11.617	11.548	0.994	1558.5
Pigott et al. (2015) (SLEC)	11.506	11.416	0.992	1511.3
Vinograd et al. (2006) (SLEC)	11.494	11.392	0.991	1505.0
Yu et al. (2011) (0GPa, 300 K, QHA-LDA)	11.540	11.420	0.990	1519.2
De La Pierre and Belmonte (2016) (Gaussian)	11.611	11.543	0.994	1556.2
<i>P</i> = 10 GPa				
Experiment, room temperature				
Yagi et al. (1992)	11.315	11.214	0.991	1435.7
Calculation, static				
This study (PBE-GGA)	11.425	11.304	0.990	1475.7
Pigott et al. (2015) (SLEC)	11.307	11.211	0.992	1433.3
<i>P</i> = 20 GPa				
Calculation, static				
This study (PBE-GGA)	11.249	11.124	0.989	1407.5
Li et al. (2007) (PW91-GGA)	11.246	11.123	0.989	1406.8
Pigott et al. (2015) (USPP-PW91-GGA)	11.251	11.115	0.988	1407.1
Pigott et al. (2015) (SLEC)	11.144	11.048	0.991	1372.1
<i>P</i> = 30 GPa				
Calculation, static				
This study (PBE-GGA)	11.100	10.979	0.989	1352.8
Li et al. (2007) (PW91-GGA)	11.098	10.976	0.989	1352.0

energy convergence criterion of  $10^{-8}$  eV. Convergence tests indicated that total energies calculated with these parameters were converged to within 0.2 meV/atom. We optimized the structure by minimizing the enthalpy at 0, 10, 20, 30 GPa and then calculated the elastic constants, described below.

For the high-temperature simulations, Brillouin zone sampling was restricted to the zone center ( $\Gamma$  point), a plane-wave cutoff of 500 eV was used and the energy convergence criterion was  $10^{-6}$  eV. Convergence tests indicated that total energies calculated with these parameters were converged to better than 1.0 meV/atom. The initial configurations for the high-temperature calculations were the optimized structures of MgSiO<sub>3</sub>-majorite from the static simulations. We performed ab initio molecular dynamics (AIMD) simulations within the NVT ensemble, making use of the Nosé thermostat (Nosé, 1984). Calculations were run at temperatures of 1000, 1500 and 2000 K and each run for a total of 6 ps, using a time-step of 1 fs. We carefully verified the stress tensors of these undeformed AIMD simulations were hydrostatic, as shown in Fig. S1.

### 2.3. Calculations of elastic properties

To calculate the elastic constants, we follow the method outlined in previous studies (Karki et al., 2001; Oganov et al., 2001; Wallace, 1972; Zhang et al., 2013). Starting from the geometry output from a static relaxation simulation or an equilibrium undeformed molecular dynamics simulation, we apply 4 types of strain: 3 axial (along each crystallographic axis) and 1 triclinic (shear strain) and calculate the resulting stresses. The magnitudes of these strains were  $\pm 0.1\%$ ,  $\pm 0.3\%$  for static calculations and  $\pm 1\%$ ,  $\pm 2\%$  for the high-temperature simulations. The isothermal elastic constants,  $C_{ijkl}^T$ , were then calculated by fitting a second-order polynomial to the strain-stress data. The isothermal elastic constants were converted to adiabatic elastic

constants,  $C_{ijkl}^S$ , using standard thermodynamically self-consistent formulae (Davies, 1974; Wallace, 1998):

$$C_{ijkl}^S = C_{ijkl}^T + \frac{TV}{C_V} b_{ij} b_{kl} \quad (1)$$

where  $C_V$  is the isochoric heat capacity and  $b_{ij} = (\partial\sigma_{ij}/\partial T)_V$  is the thermal stress tensor, which were calculated by linear-least-square fitting of internal energy and stress tensor along isochores. Based on these results, we obtained Grüneisen parameters, thermal expansivity, Voigt-Reuss-Hill bulk and shear moduli, and compressional and shear wave velocities. Uncertainties in these quantities were determined with appropriate non-Gaussian statistics via the blocking method (Flyvbjerg and Petersen, 1989). Seismic anisotropies were calculated by using MSAT (Walker and Wookey, 2012) and azimuthal anisotropy for  $V_P$  and  $V_S$  were defined as  $A_P = \frac{V_P^{max} - V_P^{min}}{V_P^{iso}} * 100$  and  $A_S = \frac{V_S^{max} - V_S^{min}}{V_S^{iso}} * 100$  respectively (Kawai and Tsuchiya, 2015).

## 3. Results and discussion

### 3.1. Lattice parameters and elastic constants

In Table 1, we compare the lattice parameters from this study and those from previous theoretical and experimental studies. Compared with the experiments, our calculated values overestimate the lattice parameters ( $a$  and  $c$ ) by  $\sim 1\%$  and volume by  $\sim 4\%$ , which is expected since GGA functionals tend to under-bind and overestimate pressure and moduli. These systematic errors were also found in previous DFT simulations using GGA, such as those from Li et al. (2007), which perfectly match our static calculations over the whole pressure range from 0 to 30 GPa. Compared with other simulations, the maximum differences are  $\sim 1\%$  in  $a$  and  $c$ , and  $\sim 4\%$  in volume, due to differences in the simulation details.

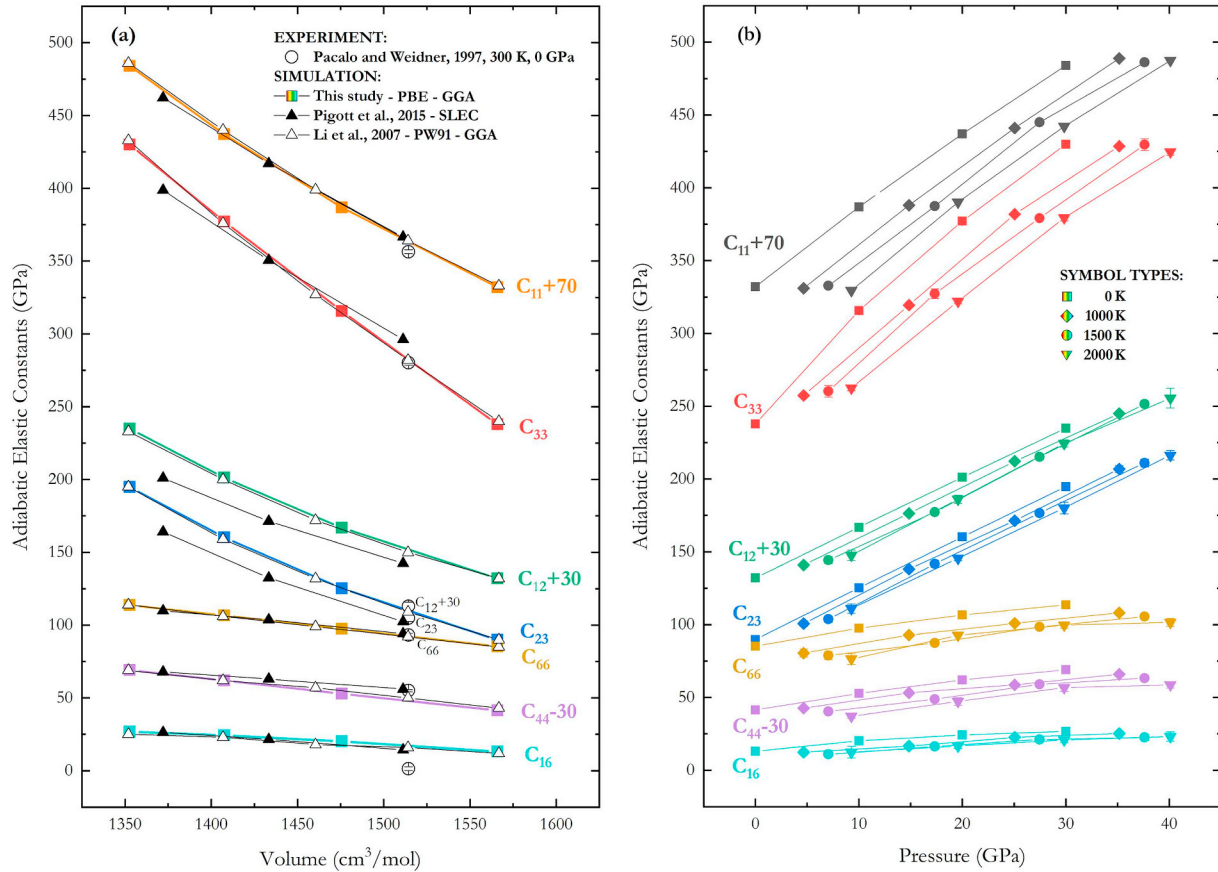


**Fig. 2.** Comparison of elastic constants at static conditions (a) and variation of elastic constants with pressure, at different temperatures (b). Colored solid symbols are our results, with uncertainties less than the sizes of the symbols, if not explicitly shown. The points are connected by straight lines to enable a better comparison with the various experimental data. Experimental data are included in (a) for comparisons: open circles with error bars are the measured values of Pacalo and Weidner (1997), while the solid and open triangles are the calculated values of Pigott et al. (2015) and Li et al. (2007), respectively. (For interpretation of the references to color in this figure legend, the reader is referred to the web version of this article.)

The raw simulated elastic constants are listed in Table S2. In Fig. 2, we show these data as a function of volume and pressure at various temperatures and compare them with currently available experimental and theoretical data. At static conditions, the results of Li et al. (2007) are in perfect agreement with our own. The elastic constants determined by Pigott et al. (2015) through static lattice-energy calculations (SLEC) generally agree well with ours, but  $C_{23}$  and  $C_{12}$  are about  $\sim 8.8\%$  and  $\sim 9.5\%$  larger than our predictions. The experimental data of Pacalo and Weidner (1997) are also in accord with our results except for  $C_{12}$  and  $C_{16}$ , which strongly deviate from the predictions of all the theoretical simulations. Compared with the results of Pacalo and Weidner (1997),  $C_{12}$  calculated in this study is  $\sim 40$  GPa larger and  $C_{16}$  is  $\sim 16$  GPa larger (Table S3).

The temperature and pressure dependence of the elastic constants are shown in Fig. 2(b).  $C_{11}$  and  $C_{33}$  increase significantly with decreasing temperature or increasing pressure. They show some non-linear pressure dependence, especially in the static calculations. This is similar to the pressure dependence of the diagonal component elastic constants in pyrope, as mentioned by Hu et al. (2016).  $C_{12}$  and  $C_{23}$  also increase strongly with the pressure, but in a more linear manner. The other elastic constants,  $C_{44}$ ,  $C_{66}$ , and  $C_{16}$ , vary less with temperature and pressure, although the non-linearity is more evident than  $C_{12}$  and  $C_{23}$ .

### 3.2. Seismic anisotropy

The seismic anisotropies of MgSiO<sub>3</sub>-majorite, based on our elastic constants and those from other studies, are shown in Fig. 3. In all cases,

the symmetry of the seismic anisotropy is not aligned with the lattice vectors. This is in contrast with crystals with cubic or orthorhombic structured symmetry (Mainprice, 2015), and caused by the finite value in  $C_{16}$ . The physical reason for this is schematically illustrated in Fig. S2, where in contrast to cubic pyrope, strain in  $a$ -direction ( $\epsilon_1$ ) in the ordered tetragonal structure causes non-zero shear stress ( $\sigma_6$ ), because the tetrahedra are connected by non-equivalent adjacent octahedra: one connects with four softer Mg octahedra and the other with four harder Si octahedra.

Our calculated seismic anisotropy, at static conditions, is in very good agreement with that of Li et al. (2007) and similar to that of Pigott et al. (2015), but does not agree with the results of Pacalo and Weidner (1997). The orientation of the pattern of anisotropy is the most prominent difference between theoretical studies and the experimental work of Pacalo and Weidner (1997). The  $C_{16}$  of Pacalo and Weidner (1997) is only 1.4 GPa, which is much smaller than all the theoretical studies. As mentioned in Li et al. (2007), the MgSiO<sub>3</sub>-majorite sample of Pacalo and Weidner (1997) may be somewhat disordered and, although the degree of disorder is unknown, this would plausibly explain the deviation here because disorder would make the two sites more similar on average.

In Fig. 3, the anisotropies from our simulations and those from Li et al. (2007) are almost the same in both  $A_p$  (8.0%:7.4%) and  $A_{Smax}$  (maximum value of  $A_S$ , 14.70%:13.07%). Compared with those of Pigott et al. (2015), there are some minor differences in both  $A_p$  (8.0%:5.1%) and  $A_{Smax}$  (14.70%:10.44%). Fig. 3(a) and (d) show that our calculated anisotropies at 0 K and 0 GPa are much larger than those measured by Pacalo and Weidner (1997) at ambient conditions. For  $A_p$

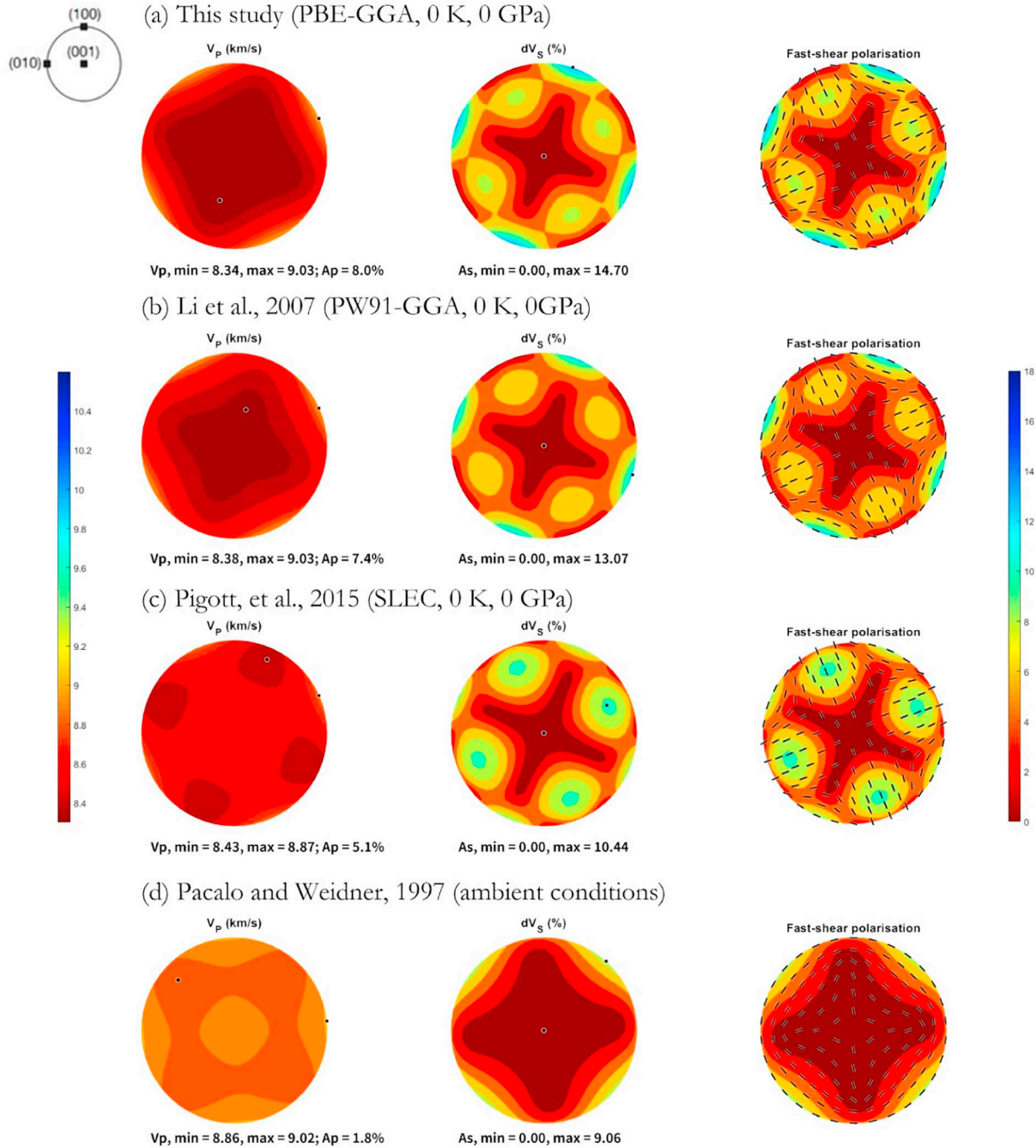


**Fig. 3.** Seismic anisotropy of  $\text{MgSiO}_3$ -majorite at 0 K and 0 GPa calculated using our elastic constants, and those of Pacalo and Weidner (1997), Pigott et al. (2015) and Li et al. (2007). The left legend shows the value range of  $V_p$  splitting (the leftmost column) and the right legend is for  $dV_s$  splitting (two columns on the right-hand side). The black dots represent maximum and minimum values in the anisotropy spheres.

it is about 4 times larger (8.0%:1.8%) and for  $A_{S_{\text{max}}}$  it is about 2 times larger (14.70%: 9.06%). In Fig. 4, we show the effects of pressure and temperature on the anisotropy of  $\text{MgSiO}_3$ -majorite. At static conditions,  $A_{S_{\text{max}}}$  increases, but  $A_p$  decreases with increasing pressure. At high-temperature conditions (1000, 1500, 2000 K),  $A_p$  and  $A_{S_{\text{max}}}$  vary slightly with temperature and both increase with pressure. At high temperatures and pressures, the values of  $A_p$  and  $A_{S_{\text{max}}}$  become almost invariant, at about 6.0% and 15.0% respectively. Fig. 4 also shows the anisotropies of pyrope (Py), grossular (Gro) and ringwoodite (Rwd) determined in previous studies. They are obviously smaller, making  $\text{MgSiO}_3$ -majorite the most anisotropic mineral in assemblages expected in the lower transition zone.

### 3.3. Elastic moduli and velocities

In Fig. 5, we plot calculated pressure and elastic moduli, as a function of volume, and compare them with previous studies. In order to make more precise comparisons with experimental data at ambient conditions, we eliminate the vibrational contribution in these experimental data following the approach proposed by Panero and Stixrude (2004). Compare to these “static” experimental data, the systematic errors from the PBE exchange-correlation functional are found to be up to  $\sim 10$  GPa in pressure,  $\sim 20$  GPa in isothermal bulk modulus and  $\sim 20$  GPa in shear modulus. We applied a rescaling method to eliminate these systematic errors (Zhang and Liu, 2015; Zhang et al., 2018; Zhang et al., 2013)

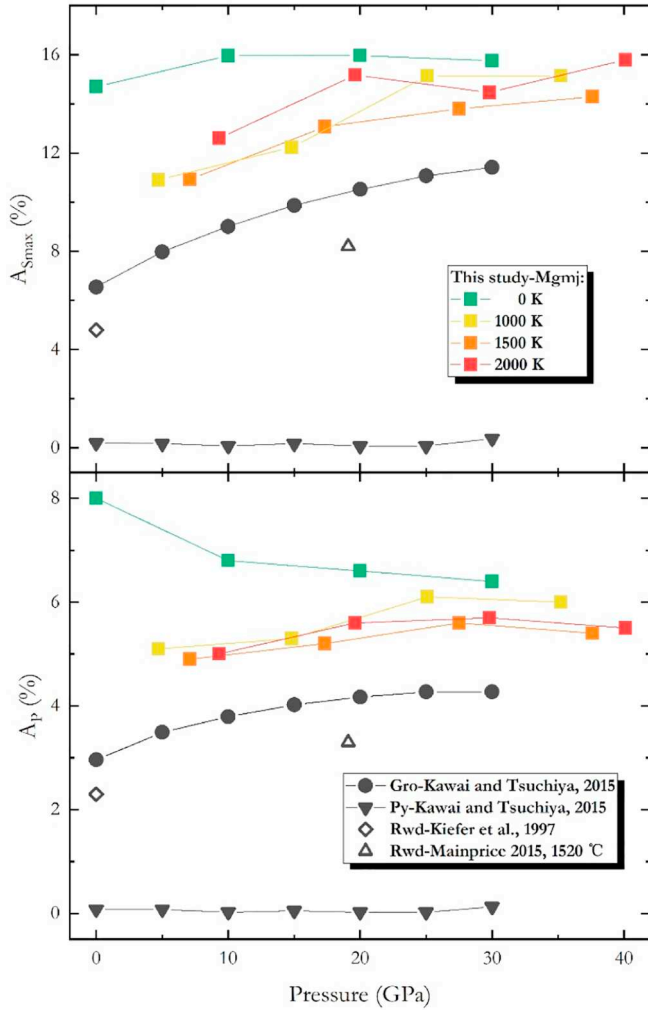


**Fig. 4.** The azimuthal anisotropies of MgSiO<sub>3</sub>-majorite and other major phases in the transition zone in (a)  $A_{Smax}$  and (b)  $A_p$ . Lines that connect data points are simple straight lines that are used to show the trend. Solid colored squares are our data for MgSiO<sub>3</sub>-majorite, dark circles and triangles represent theoretical data of pyrope and grossular at static conditions, respectively. Open diamonds represent experimental data for ringwoodite at ambient conditions. Open triangles are experimental data for ringwoodite at 1793 K, which were obtained by extrapolating experimental values (Jackson et al., 2000; Sinogeikin et al., 1998; Sinogeikin et al., 2001; Weidner et al., 1984) to a depth of 550 km. (For interpretation of the references to color in this figure legend, the reader is referred to the web version of this article.)

$$M(V, T) = \frac{K_0^{exp}}{K_0^{PBE}} M^{PBE} \left( V \frac{V_0^{PBE}}{V_0^{exp}} \right) + \Delta M^{PBE}(V, T) \quad (2)$$

where  $M$  is the property to be rescaled ( $P$ ,  $K$  or  $G$ ), subscript 0 refers to properties at zero pressure and static conditions, quantities lacking temperature dependence are athermal (static),  $K$  is the isothermal bulk modulus, and  $\Delta$  denotes the change in the quantity from static conditions to the temperature of interest, i.e.  $\Delta M^{PBE}(V, T) = M^{PBE}(V, T) - M^{PBE}(V)$ . The parameters in Eq. (2) are  $V_0^{exp} = 112.8 \text{ cm}^3/\text{mol}$ ,  $K_0^{exp} = 168.6 \text{ GPa}$  and  $V_0^{PBE} = 117.9 \text{ cm}^3/\text{mol}$ ,  $K_0^{PBE} = 146.9 \text{ GPa}$ . We report our final corrected data in Table 2. Based on these data, we refitted the third-order Birch-Murnaghan-Mie-Grüneisen model proposed by Stixrude and Lithgow-Bertelloni (2005, 2011). The new parameters for the thermoelastic model of MgSiO<sub>3</sub>-majorite are listed in the caption of Table 2.

After eliminating systematic errors, our results are in good agreement with the experimental data within their uncertainties or the

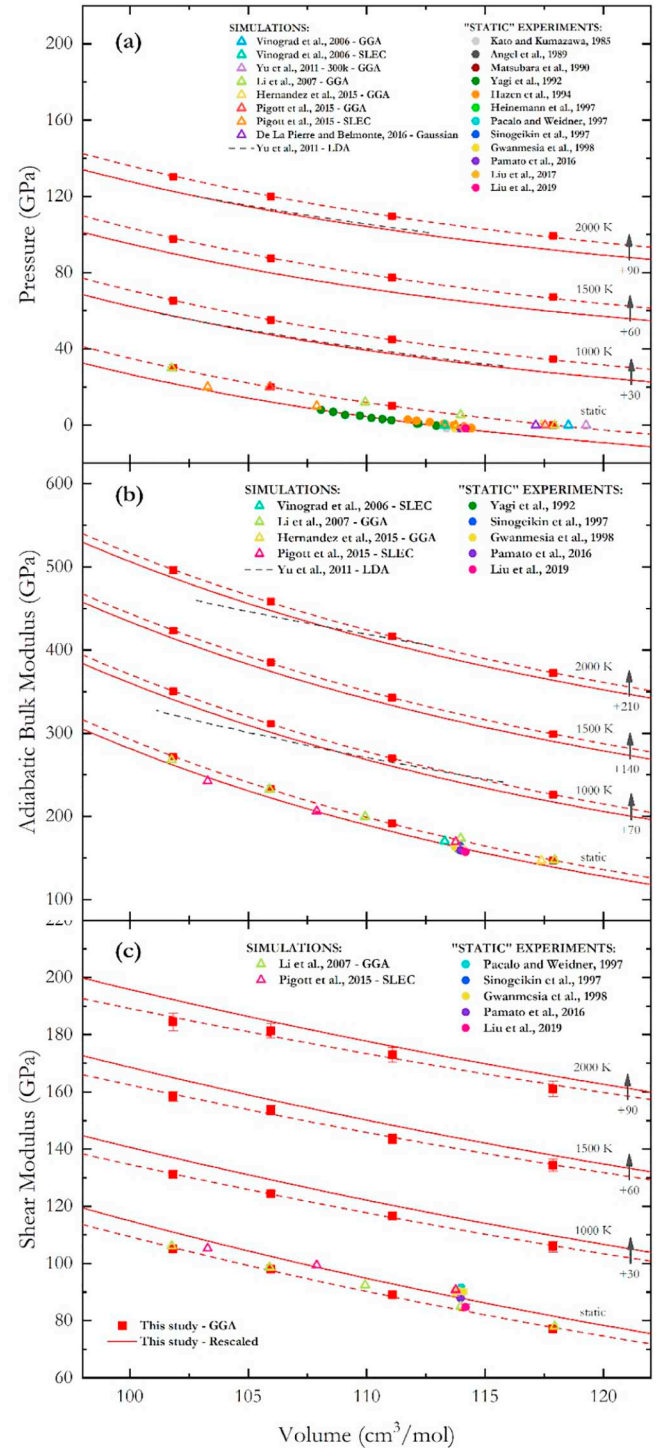


**Fig. 5.** Comparisons between our calculated (a) pressure, (b) adiabatic bulk modulus and (c) shear modulus as a function of volume, and the results of other studies. Red dashed lines are fits to our calculated results (red solid squares), and solid lines are fits to our rescaled results. Other theoretical data are denoted by colored open triangles. Experimental data at room temperature have been corrected to the “static” condition (see text) and are denoted by colored solid circles. Some error bars cannot be observed due to small values or lack of reporting in their original works. (For interpretation of the references to color in this figure legend, the reader is referred to the web version of this article.)

scattering of different datasets. Compared with previous simulations, the volumes of Yu et al. (2011) at 300 K are a little higher than our results (Fig. 5(a)) due to small thermal effects. The results from the

**Table 2**

Elastic moduli of MgSiO<sub>3</sub>-majorite from static conditions to high temperatures and pressures, rescaled from the raw simulation results in this study (listed in Table S2). Parameters for the thermodynamic model of [Stixrude and Lithgow-Bertelloni \(2011\)](#) refitted from these results are:  $T_0 = 300$  K,  $V_0 = 114.1$  cm<sup>3</sup>/mol,  $K_0 = 163.6$  GPa,  $G_0 = 86.4$  GPa,  $K_0' = 4.44$ ,  $G_0' = 1.16$ ,  $\gamma_0 = 1.08$ ,  $q_0 = 0.48$ ,  $\eta_{so} = 0.76$ ,  $\theta_0 = 822.5$  K.

T (K)	0				1000				1500				2000			
$P$ (GPa)	-6.8	2.6	12.2	21.8	-2.1	7.5	17.3	26.9	0.3	10.0	19.6	29.4	2.5	12.2	22.0	31.9
$V$ (Å <sup>3</sup> )	117.9	111.1	106.0	101.8	117.9	111.1	106.0	101.8	117.9	111.1	106.0	101.8	117.9	111.1	106.0	101.8
$K_T$ (GPa)	138.0	182.0	222.8	261.6	141.8	185.3	226.5	265.0	142.2	185.8	227.6	265.5	143.5	187.0	228.6	266.0
$K_S$ (GPa)					147.0	190.6	231.6	270.1	149.8	193.1	235.2	273.0	153.3	196.8	238.2	275.9
$G$ (GPa)	80.3	93.2	103.0	110.8	79.1	90.8	99.3	106.9	77.7	87.8	98.6	104.2	74.2	87.1	96.4	100.3

$V$  means volumes of unit cell. The uncertainties are within 0.1 GPa for pressure and generally within 3% for bulk and shear moduli.

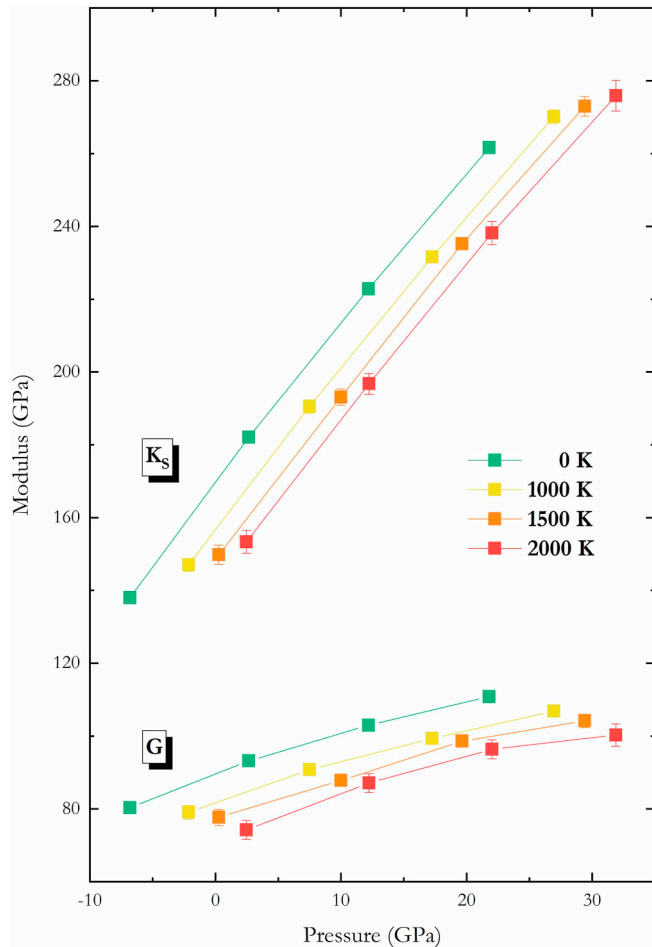


**Fig. 6.** Pressure-dependence of adiabatic bulk and shear moduli. Colored solid symbols with error bars are our rescaled data. For most data points the error bars are smaller than the symbol size. (For interpretation of the references to color in this figure legend, the reader is referred to the web version of this article.)

SLEC of [Vinograd et al. \(2006\)](#) and [Pigott et al. \(2015\)](#) are consistent with our rescaled data but at high pressures, deviations are noticeable, up to 13.5 GPa (~5.6%) in bulk modulus and 6.7 GPa (~6.3%) in shear modulus. At high temperatures, we find apparent good agreement between our rescaled results and those of [Yu et al. \(2011\)](#) over the whole pressure range, but more careful analysis (Fig. S3) reveals some subtle deviations. These may be due the neglect of anharmonicity in the lattice dynamics simulations of [Yu et al. \(2011\)](#), which is included in our molecular dynamics simulations. [Oganov et al. \(2000\)](#) showed that this can lead to overestimation of the thermal expansion coefficients and

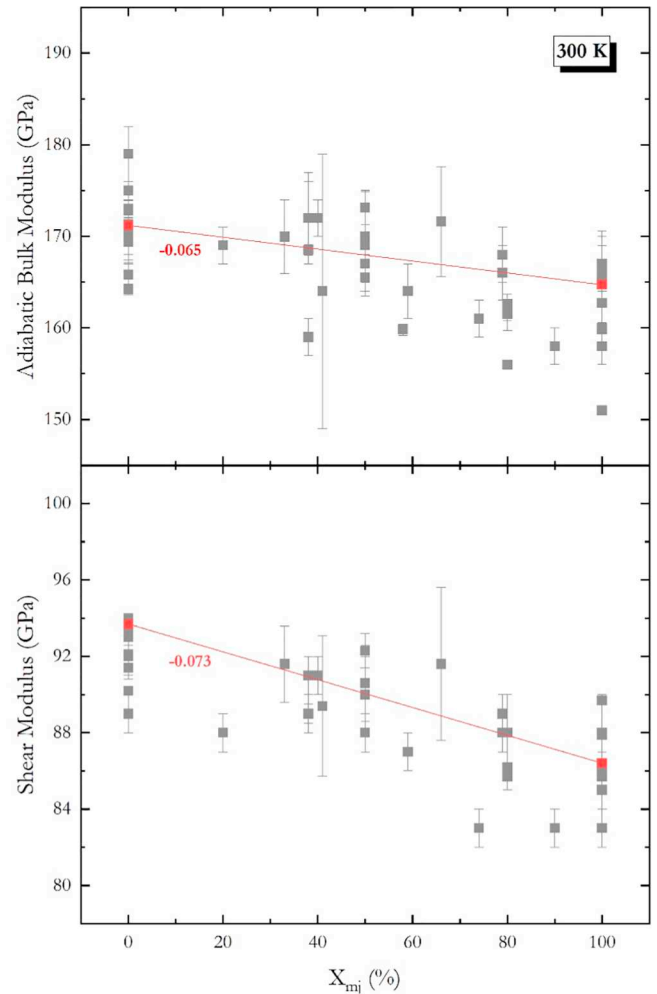


**Fig. 7.** (a) Adiabatic bulk modulus and (b) shear modulus as a function of MgSiO<sub>3</sub>-majorite content along the majorite-pyrope join, at 300 K and ambient pressure. In (a) and (b), red solid squares with error bars are our calculated values. Numbers near straight lines are gradients. Grey solid squares with error bars are experimental data ([Babuska et al., 1978](#); [Bass and Kanzaki, 1990](#); [Chen et al., 1999](#); [Conrad et al., 1999](#); [Gwanmesia et al., 1998](#); [Gwanmesia et al., 2000](#); [Gwanmesia et al., 2009](#); [Gwanmesia et al., 2006](#); [Hazen and Finger, 1989](#); [Isaak and Graham, 1976](#); [Kavner et al., 2000](#); [Leger et al., 1990](#); [Leitner et al., 1980](#); [Levien et al., 1978](#); [Liu et al., 2000](#); [Liu et al., 2019](#); [Liu et al., 2015](#); [Morishima et al., 1999](#); [Pacalo and Weidner, 1997](#); [Pamato et al., 2016](#); [Rigden et al., 1994](#); [Sato et al., 1978](#); [Sinogeikin and Bass, 2000, 2002a, 2002b](#); [Sinogeikin et al., 1997](#); [Wang et al., 1998](#); [Wang and Ji, 2001](#); [Yagi et al., 1987](#); [Yeganehhaeri et al., 1990](#); [Zhang et al., 1999](#); [Zou et al., 2012](#)). (For interpretation of the references to color in this figure legend, the reader is referred to the web version of this article.)

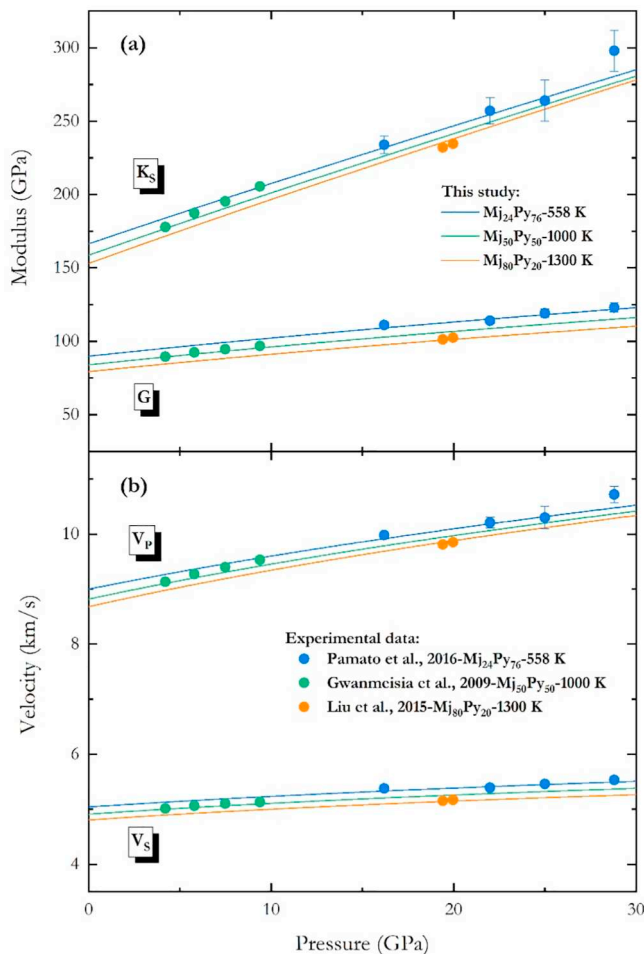


**Fig. 8.** Calculated values of (a)  $K_s$  and  $G$ , (b)  $V_p$  and  $V_s$  along the Mj-Py join, compared with experimental results at high temperatures and pressures.

Grüneisen parameters at high temperatures, which we also find (Fig. S4). At a fixed volume, overestimation of the thermal expansion coefficient, results in an overestimation of pressure, leading to difference in calculated  $P$ - $V$  curves and, in turn bulk moduli (up to over 30 GPa for isothermal bulk modulus and over 20 GPa for the adiabatic bulk modulus), as shown in Fig. S3.

In Fig. 6, we show the adiabatic moduli of  $\text{MgSiO}_3$ -majorite at various pressures and temperatures. The bulk modulus significantly increases with pressure, doubling when going from 0 to 30 GPa. The shear modulus also increases noticeably by up to 40 GPa over the same pressure range. In common with the elastic constants, both moduli show some non-linear pressure-dependence. The bulk and shear modulus exhibit strong temperature dependence. Increasing the temperature by 2000 K, causes the adiabatic bulk and shear moduli to decrease linearly by 22–26 GPa and 16–18 GPa, respectively.

As an important solid solution in the transition zone, the majorite-pyropite join has been the focus of many experimental studies (Bass and Kanzaki, 1990; Gwanmesia et al., 2000; Gwanmesia et al., 2009; Hunt et al., 2010; Liu et al., 2000; Liu et al., 2019; Liu et al., 2015; Morishima et al., 1999; Pamato et al., 2016; Rigden et al., 1994; Sinogeikin and Bass, 2002a, 2002b; Sinogeikin et al., 1997; Wang et al., 1998; Yagi et al., 1987; Yeganehhaeri et al., 1990). We plot the bulk and shear moduli from these experimental studies against the composition in Fig. 7, together with those calculated from our results for  $\text{MgSiO}_3$ -majorite and those from the predictions of Stixrude and Lithgow-Bertelloni (2011) for  $\text{Mg}_3\text{Al}_2[\text{SiO}_4]_3$ -pyrope. Assuming linear mixing, as suggested by previous studies (Bass and Kanzaki, 1990; Gwanmesia et al., 2000; Liu et al., 2019), we find the linear equations of

$K_s = 171.2 - 0.065 * X_{Mj}$  and  $G = 93.7 - 0.073 * X_{Mj}$ , determined by our calculations, agree with the experiments within the uncertainties and scattering of the experimental data. We calculate  $K_s$ ,  $G$ ,  $V_p$  and  $V_s$  for majorite-pyropite solid solutions at high temperatures and pressures (Fig. 8), which show good agreement with the measured values of Gwanmesia et al. (2009), Liu et al. (2015) and Pamato et al. (2016).

#### 4. Implications for interpreting the seismic observations in the transition zone

The thermoelastic model of  $\text{MgSiO}_3$ -majorite obtained in this study has been used to determine the seismic velocities of pyrolite, basalt, and harzburgite mineral assemblages, with the bulk chemical compositions reported by Workman and Hart (2005), Baker and Beckett (1999) and compiled by Xu et al. (2008), as listed in Table S4. Besides  $\text{MgSiO}_3$ -majorite, we included another 46 end-members and 21 phases, using the parameters listed in Table A1 of Stixrude and Lithgow-Bertelloni (2011), except for  $\text{MgSiO}_3$ -perovskite (bridgmanite) for which we used the parameters optimized by Zhang et al. (2013) and cubic  $\text{CaSiO}_3$ -perovskite for which we used the parameters recently re-determined by Thomson et al. (2019). Note that for the garnet phase, in which majorite resides, we have included five typical end-members (pyrope, almandine, grossular, Mg-Majorite and Jd-Majorite, as listed in Table A1 of Stixrude and Lithgow-Bertelloni (2011)). So the effect of iron in the garnet solid solution has only been accounted for on the dodecahedral sites. The adiabatic geotherm with a potential temperature of 1500 K leads to a temperature range of ~1690–1820 K in the transition zone, which is within the estimate of  $1773 \pm 100$  K at a depth of 410 km suggested by Frost (2008). With these inputs, we obtained the phase proportions of pyrolite, basalt and harzburgite by minimizing the Gibbs free energy, as proposed by Stixrude and Lithgow-Bertelloni (2011). Using the properties of individual phases, we calculated the seismic velocities of equilibrium mineral assemblages through Voigt-Reuss-Hill averaging.

In Fig. 9, we compare the velocities predicted for a pyrolite mineral assemblage with several seismic models. It shows that the agreement is fair to good for the global seismic models (Dziewonski and Anderson, 1981; Kennett et al., 1995) in the upper transition zone, considering the uncertainties in the seismic observations and the possible uncertainty in temperature (Xu et al., 2008). The agreement extends to the lower transition zone, as compared with the local seismic model of TNA2, which was proposed by Wang et al., 2014 for the transition zone beneath the East Pacific Rise.

Compared with PREM and AK135, the equilibrium pyrolite model seems to predict too low shear-wave velocities with increasing depth from about 520 km. Due to the sluggish chemical diffusivity of mantle materials ( $10^{-14}$ – $10^{-16}$   $\text{m}^2\text{s}^{-1}$ ) in the solid state (Farber et al., 1994; Hofmann and Hart, 1978; Yamazaki et al., 2000), mechanically mixed mantle models are considered by a number of previous studies (Allègre and Turcotte, 1986; Hofmann and Hart, 1978; Ritsema et al., 2009; Xu et al., 2008). Inspired by these studies, we separately calculated the densities and seismic velocities of basalt and harzburgite compositions, and linearly combined them with 18% basalt and 82% harzburgite to get the densities and seismic velocities of the modeled mechanical mixture proposed by Xu et al. (2008). The density of the mechanical mixture is, just like pyrolite, in good agreement with PREM and AK135, but its velocities are found to be in better agreement with PREM than equilibrium pyrolite, as shown in Fig. 9.

Similar to the comparisons in Fig. 9, a number of previous studies support the aggregation of harzburgite in the lower transition zone (Irfune et al., 2008; Nakagawa and Buffett, 2005). This would be important for the anisotropy of the lower transition zone. As shown in Fig. S5, the amount of  $\text{MgSiO}_3$ -majorite in the garnet phase of harzburgite is significantly higher than that in pyrolite and basalt, and according to Sinogeikin et al. (1997), the solid solution of majorite-pyropite maintains the tetragonal structure when  $\text{MgSiO}_3$ -majorite accounts for 70% or

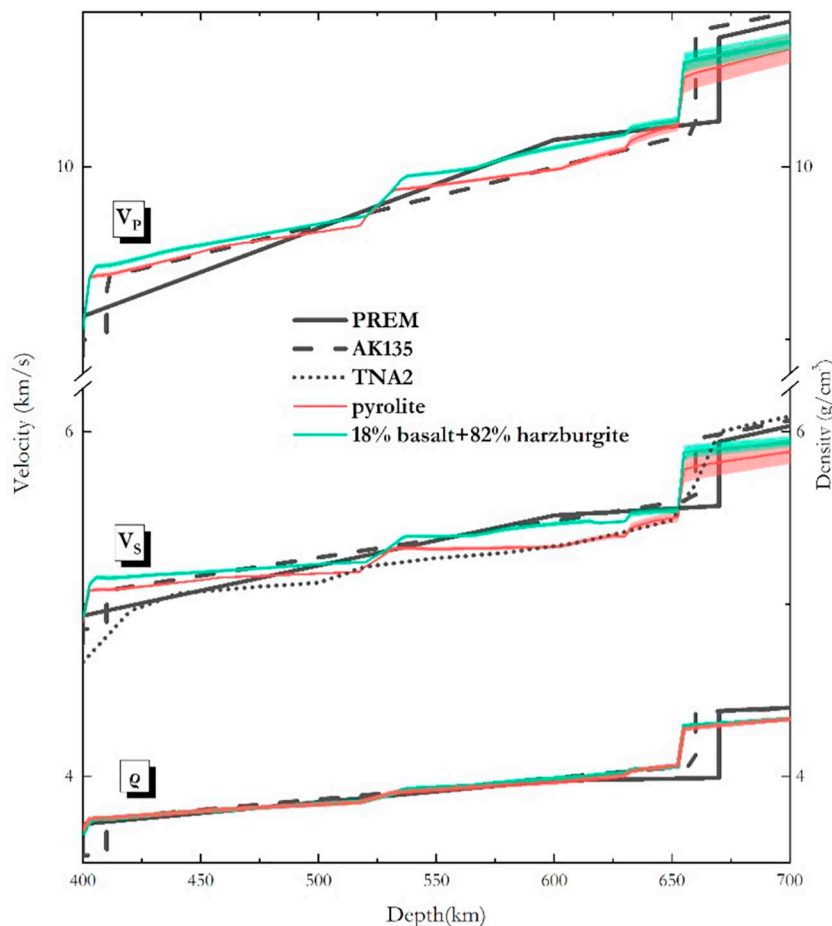


**Fig. 9.** Comparisons of seismic wave velocities and densities among our models (colored solid lines), global models: PREM (dark grey solid line) and AK135 (dark grey dashed line), and local model TNA2 (dark grey dot line). Our models are along the adiabatic geotherm with a potential temperature of 1500 K. Colored shaded zone are Voigt-Reuss bounds of our models. (For interpretation of the references to color in this figure legend, the reader is referred to the web version of this article.)

higher. The noticeable anisotropy, as revealed in Figs. 3 and 4, would, therefore, contribute to the anisotropy in the lower transition zone, which may be very small on a global scale (Huang et al., 2019), but observable, at a local scale, in heterogeneous zones near the subducting slabs (Lynner and Long, 2015).

## 5. Conclusions

We have performed first principles calculations to determine the thermoelastic properties of  $\text{MgSiO}_3$ -majorite over a wide range of temperatures and pressures. The elastic constants for  $\text{MgSiO}_3$ -majorite show noticeable non-linear pressure dependence. The anisotropies in  $V_P$  and  $V_S$  of  $\text{MgSiO}_3$ -majorite are found to be higher than the other major minerals such as pyrope, grossular, and ringwoodite, making  $\text{MgSiO}_3$ -majorite the most anisotropic mineral in assemblages expected in the lower transition zone. With careful elimination of the systematic errors in the simulation results, the determined elastic properties are shown to be in good agreement with the limited available experimental measurements for  $\text{MgSiO}_3$ -majorite and the majorite-pyrope join. Based on the high quality data obtained in this study, we have proposed an optimized thermodynamic model for  $\text{MgSiO}_3$ -majorite that is able to accurately predict its elastic properties at simultaneously high temperatures and pressures.

The thermoelastic properties of  $\text{MgSiO}_3$ -majorite determined in this study were used to predict the seismic velocities of pyrolite, harzburgite, and basalt mineral assemblages, at the conditions of the transition zone. These showed that, on a global scale, the seismic velocities of the upper transition zone are consistent with a pyrolite-like composition, but this equilibrium assemblage may only extend to the lower transition zone in local regions. Compared with global seismic models, better agreement with PREM than AK135 implies that the lower transition

zone is more consistent with an 18% basalt and 82% harzburgite mechanical mixture. The aggregation of harzburgite in the lower transition zone would lead to a much higher  $\text{MgSiO}_3$ -majorite content in the garnet phase and cause a cubic-tetragonal phase transition in garnet, which may result in non-negligible anisotropy in the lower transition zone.

## CRediT authorship contribution statement

**Yancheng Lou:** Investigation, Writing - original draft. **Stephen Stackhouse:** Methodology, Writing - review & editing. **Andrew M. Walker:** Methodology, Writing - review & editing. **Zhigang Zhang:** Conceptualization, Methodology, Supervision, Writing - review & editing.

## Declaration of competing interest

The authors declare that they have no known competing financial interests or personal relationships that could have appeared to influence the work reported in this paper.

## Acknowledgments

We are thankful for helpful discussions with Profs. Yigang Zhang, Guangjun Guo, and Jian Wang, and to Prof. Lars Stixrude for kindly providing their HeFESTo results. We are grateful to two anonymous reviewers for their helpful comments and to Prof. Kei Hirose for his handling our manuscript. This work was supported by the Strategic Priority Research Program (B) of the Chinese Academy of Sciences (#XDB18000000) and by the National Natural Science Foundation of

China (#41590620). Simulations were carried out on the computational facilities in the Computer Simulation Lab of IGGCAS and Tianhe-2 at the National Supercomputer Center of China (NSCC) in Guangzhou. The collaboration leading to this paper was made possible by the U.K.-Sino Centre for Earth and Planetary Science. AMW was partially supported by the Natural Environment Research Council (NE/M000044/1).

## Data availability

The data for this paper can be found in the supplementary and more extended raw data are available on request.

## Appendix A. Supplementary data

Supplementary data to this article can be found online at <https://doi.org/10.1016/j.pepi.2020.106491>.

## References

- Allègre, C.J., Turcotte, D.L., 1986. Implications of a two-component marble-cake mantle. *Nature* 323 (6084), 123.
- Angel, R.J., Finger, L.W., Hazen, R.M., Kanzaki, M., Weidner, D.J., Liebermann, R.C., Veblen, D.R., 1989. Structure and twinning of single-crystal MgSiO<sub>3</sub> garnet synthesized at 17 GPa and 1800-degrees-C. *Am. Mineral.* 74 (3–4), 509–512.
- Babuska, V., Fiala, J., Kumazawa, M., Ohno, I., Sumino, Y., 1978. Elastic properties of garnet solid-solution series. *Phys. Earth Planet. Inter.* 16 (2), 157–176. [https://doi.org/10.1016/0031-9201\(78\)90086-9](https://doi.org/10.1016/0031-9201(78)90086-9).
- Baker, M.B., Beckett, J.R., 1999. The origin of abyssal peridotites: a reinterpretation of constraints based on primary bulk compositions. *Earth Planet. Sci. Lett.* 171 (1), 49–61.
- Bass, J.D., Kanzaki, M., 1990. Elasticity of a majorite-pyrope solid-solution. *Geophys. Res. Lett.* 17 (11), 1989–1992. <https://doi.org/10.1029/GL017i011p01989>.
- Blöchl, P.E., 1994. Projector augmented-wave method. *Phys. Rev. B* 50 (24), 17953.
- Chen, G.L., Cooke, J.A., Gwanmesia, G.D., Liebermann, R.C., 1999. Elastic wave velocities of Mg<sub>3</sub>Al<sub>2</sub>Si<sub>3</sub>O<sub>12</sub>-pyrope garnet to 10 GPa. *Am. Mineral.* 84 (3), 384–388.
- Conrad, P.G., Zha, C.S., Mao, H.K., Hemley, R.J., 1999. The high-pressure, single-crystal elasticity of pyrope, grossular, and andradite. *Am. Mineral.* 84 (3), 374–383.
- Davies, G.F. (1974). Effective elastic-moduli under hydrostatic stress. 1. Quasi-harmonic theory. *J. Phys. Chem. Solids*, 35(11), 1513–1520. doi:[https://doi.org/10.1016/S0022-3697\(74\)80279-9](https://doi.org/10.1016/S0022-3697(74)80279-9).
- De La Pierre, M., Belmonte, D., 2016. Ab initio investigation of majorite and pyrope garnets: lattice dynamics and vibrational spectra. *Am. Mineral.* 101 (1–2), 162–174. <https://doi.org/10.2138/am-2016-5382>.
- Dziewonski, A.M., Anderson, D.L., 1981. Preliminary reference earth model. *Phys. Earth Planet. Inter.* 25 (4), 297–356. [https://doi.org/10.1016/0031-9201\(81\)90046-7](https://doi.org/10.1016/0031-9201(81)90046-7).
- Farber, D.L., Williams, Q., Ryerson, F.J., 1994. Diffusion in Mg<sub>2</sub>SiO<sub>4</sub> polymorphs and chemical heterogeneity in the mantle transition zone. *Nature* 371 (6499), 693.
- Flyvbjerg, H., Petersen, H.G., 1989. Error-estimates on averages of correlated data. *J. Chem. Phys.* 91 (1), 461–466. <https://doi.org/10.1063/1.457480>.
- Frost, D.J., 2008. The upper mantle and transition zone. *Elements* 4 (3), 171–176. <https://doi.org/10.2113/Gselements.4.3.171>.
- Gwanmesia, G.D., Chen, G.L., Liebermann, R.C., 1998. Sound velocities in MgSiO<sub>3</sub>-garnet to 8 GPa. *Geophys. Res. Lett.* 25 (24), 4553–4556. <https://doi.org/10.1029/1998gl900189>.
- Gwanmesia, G.D., Liu, J., Chen, G., Kesson, S., Rigden, S.M., Liebermann, R.C., 2000. Elasticity of the pyrope (Mg<sub>3</sub>Al<sub>2</sub>Si<sub>3</sub>O<sub>12</sub>)-majorite (MgSiO<sub>3</sub>) garnets solid solution. *Phys. Chem. Miner.* 27 (7), 445–452. <https://doi.org/10.1007/s002699900054>.
- Gwanmesia, G.D., Zhang, J.Z., Darling, K., Kung, J., Li, B.S., Wang, L.P., ... Liebermann, R.C., 2006. Elasticity of polycrystalline pyrope (Mg<sub>3</sub>Al<sub>2</sub>Si<sub>3</sub>O<sub>12</sub>) to 9 GPa and 1000 degrees C. *Physics of the Earth and Planetary Interiors* 155 (3–4), 179–190. <https://doi.org/10.1016/j.pepi.2005.10.008>.
- Gwanmesia, G.D., Wang, L.P., Triplett, R., Liebermann, R.C., 2009. Pressure and temperature dependence of the elasticity of pyrope-majorite [Py(60)Mj(40) and Py(50)Mj(50)] garnets solid solution measured by ultrasonic interferometry technique. *Phys. Earth Planet. Inter.* 174 (1–4), 105–112. <https://doi.org/10.1016/j.pepi.2008.07.029>.
- Hazen, R.M., Finger, L.W., 1989. High-pressure crystal-chemistry of andradite and pyrope - revised procedures for high-pressure diffraction experiments. *Am. Mineral.* 74 (3–4), 352–359.
- Hazen, R.M., Downs, R.T., Conrad, P.G., Finger, L.W., Gasparik, T., 1994. Comparative compressibilities of majorite-type garnets. *Phys. Chem. Miner.* 21 (5), 344–349.
- Heinemann, S., Sharp, T.G., Seifert, F., Rubie, D.C., 1997. The cubic-tetragonal phase transition in the system majorite (Mg<sub>4</sub>Si<sub>4</sub>O<sub>12</sub>) pyrope (Mg<sub>3</sub>Al<sub>2</sub>Si<sub>3</sub>O<sub>12</sub>), and garnet symmetry in the Earth's transition zone. *Phys. Chem. Miner.* 24 (3), 206–221. <https://doi.org/10.1007/s002690050034>.
- Hernandez, E.R., Brodholt, J., Alfe, D., 2015. Structural, vibrational and thermodynamic properties of Mg<sub>2</sub>SiO<sub>4</sub> and MgSiO<sub>3</sub> minerals from first-principles simulations. *Phys. Earth Planet. Inter.* 240, 1–24. <https://doi.org/10.1016/j.pepi.2014.10.007>.
- Hofmann, A., Hart, S., 1978. An assessment of local and regional isotopic equilibrium in the mantle. *Earth Planetary Science Letters* 38 (1), 44–62.
- Hohenberg, P., Kohn, W., 1964. Inhomogeneous electron gas. *Phys. Rev.* 136 (3B), B864.
- Hu, Y., Wu, Z.Q., Dera, P.K., Bina, C.R., 2016. Thermodynamic and elastic properties of pyrope at high pressure and high temperature by first-principles calculations. *Journal of Geophysical Research-Solid Earth* 121 (9), 6462–6476. <https://doi.org/10.1002/2016jb013026>.
- Huang, Q., Schmerr, N., Waszek, L., Beghein, C., 2019. Constraints on seismic anisotropy in the mantle transition zone from long-period SS precursors. *Journal of Geophysical Research: Solid Earth* 124 (7), 6779–6800.
- Hunt, S.A., Dobson, D.P., Li, L., Weidner, D.J., Brodholt, J.P., 2010. Relative strength of the pyrope-majorite solid solution and the flow-law of majorite containing garnets. *Phys. Earth Planet. Inter.* 179 (1–2), 87–95. <https://doi.org/10.1016/j.pepi.2009.12.001>.
- Irifune, T., Higo, Y., Inoue, T., Kono, Y., Ohfuji, H., Funakoshi, K., 2008. Sound velocities of majorite garnet and the composition of the mantle transition region. *Nature* 451 (7180), 814.
- Isaak, D.G., Graham, E.K., 1976. Elastic properties of an almandine spessartine garnet and elasticity in garnet solid-solution series. *J. Geophys. Res.* 81 (14), 2483–2489. <https://doi.org/10.1029/JB081i014p02483>.
- Jackson, J.M., Sinogeikin, S.V., Bass, J.D., 2000. Sound velocities and elastic properties of  $\gamma$ -Mg<sub>2</sub>SiO<sub>4</sub> to 873 K by Brillouin spectroscopy. *Am. Mineral.* 85 (2), 296–303.
- Karki, B.B., Stixrude, L., Wentzcovitch, R.M., 2001. High-pressure elastic properties of major materials of Earth's mantle from first principles. *Rev. Geophys.* 39 (4), 507–534. <https://doi.org/10.1029/2000rg000088>.
- Kato, T., Kumazawa, M., 1985. Garnet phase of MgSiO<sub>3</sub> filling the pyroxene ilmenite gap at very high-temperature. *Nature* 316 (6031), 803–805. <https://doi.org/10.1038/316803a0>.
- Kavner, A., Sinogeikin, S.V., Jeanloz, R., Bass, J.D., 2000. Equation of state and strength of natural majorite. *Journal of Geophysical Research-Solid Earth* 105 (B3), 5963–5971. <https://doi.org/10.1029/1999jb900374>.
- Kawai, K., Tsuchiya, T., 2015. Elasticity and phase stability of pyrope garnet from ab initio computation. *Physics of the Earth Planetary Interiors* 240, 125–131.
- Kennett, B.L.N., Engdahl, E.R., Buland, R., 1995. Constraints on seismic velocities in the earth from travel-times. *Geophys. J. Int.* 122 (1), 108–124. <https://doi.org/10.1111/j.1365-246X.1995.tb03540.x>.
- Kohn, W., Sham, L.J., 1965. Self-consistent equations including exchange and correlation effects. *Phys. Rev.* 140 (4A), A1133.
- Kresse, G., Furthmüller, J., 1996a. Efficiency of ab-initio total energy calculations for metals and semiconductors using a plane-wave basis set. *Comput. Mater. Sci.* 6 (1), 15–50.
- Kresse, G., Furthmüller, J., 1996b. Efficient iterative schemes for ab initio total-energy calculations using a plane-wave basis set. *Phys. Rev. B* 54 (16), 11169–11186. <https://doi.org/10.1103/PhysRevB.54.11169>.
- Kresse, G., Hafner, J., 1993. Ab initio molecular dynamics for liquid metals. *Phys. Rev. B* 47 (1), 558.
- Kresse, G., Joubert, D., 1999. From ultrasoft pseudopotentials to the projector augmented-wave method. *Phys. Rev. B* 59 (3), 1758–1775. <https://doi.org/10.1103/PhysRevB.59.1758>.
- Leger, J.M., Redon, A.M., Chateau, C., 1990. Compressions of synthetic pyrope, spessartine and uvarovite garnets up to 25-GPa. *Phys. Chem. Miner.* 17 (2), 161–167.
- Leitner, B.J., Weidner, D.J., Liebermann, R.C., 1980. Elasticity of single-crystal pyrope and implications for garnet solid-solution series. *Phys. Earth Planet. Inter.* 22 (2), 111–121. [https://doi.org/10.1016/0031-9201\(80\)90052-7](https://doi.org/10.1016/0031-9201(80)90052-7).
- Levien, L., Prewitt, C.T., Weidner, D.J., 1978. Comparison of determinations of bulk moduli for pyrope. *Transactions-American Geophysical Union* 59 (12), 1180.
- Li, L., Weidner, D.J., Brodholt, J., Price, G.D., 2007. The effect of cation-ordering on the elastic properties of majorite: an ab initio study. *Earth Planet. Sci. Lett.* 256 (1–2), 28–35. <https://doi.org/10.1016/j.epsl.2007.01.008>.
- Liu, J., Chen, G.L., Gwanmesia, G.D., Liebermann, R.C., 2000. Elastic wave velocities of pyrope-majorite garnets (Py(62)Mj(38) and Py(50)Mj(50)) to 9 GPa. *Phys. Earth Planet. Inter.* 120 (1–2), 153–163. [https://doi.org/10.1016/S0031-9201\(00\)00152-7](https://doi.org/10.1016/S0031-9201(00)00152-7).
- Liu, Z.D., Irifune, T., Greaux, S., Arimoto, T., Shinmei, T., Higo, Y., 2015. Elastic wave velocity of polycrystalline Mj(80)Py(20) garnet to 21 GPa and 2,000 K. *Phys. Chem. Miner.* 42 (3), 213–222. <https://doi.org/10.1007/s00269-014-0712-y>.
- Liu, Z.D., Du, W., Shinmei, T., Greaux, S., Zhou, C.Y., Arimoto, T., Kunimoto, T., Irifune, T., 2017. *Phys. Chem. Miner.* 44 (4), 237–245. <https://doi.org/10.1007/s00269-016-0852-3>.
- Liu, Z.D., Greaux, S., Cai, N., Siersch, N., Ballaran, T.B., Irifune, T., Frost, D.J., 2019. Influence of aluminum on the elasticity of majorite-pyrope garnets. *Am. Mineral.* 104 (7), 929–935. <https://doi.org/10.2138/am-2019-6771>.
- Lynner, C., Long, M.D., 2015. Heterogeneous seismic anisotropy in the transition zone and uppermost lower mantle: evidence from South America, Izu-Bonin and Japan. *Geophys. J. Int.* 201 (3), 1545–1552.
- Mainprice, D. (2015). 2.20—Seismic anisotropy of the deep earth from a mineral and rock physics perspective. *Treatise on Geophysics*. Elsevier, Oxford, 487–538.
- Matsubara, R., Toraya, H., Tanaka, S., & Sawamoto, H. (1990). Precision lattice-parameter determination of (Mg,Fe)SiO<sub>3</sub> tetragonal garnets. *Science*, 247(4943), 697–699. doi:<https://doi.org/10.1126/science.247.4943.697>.
- Morishima, H., Ohtani, E., Kato, T., Kubo, T., Suzuki, A., Kikegawa, T., Shimomura, O., 1999. The high-pressure and temperature equation of state of a majorite solid solution in the system of Mg<sub>4</sub>Si<sub>4</sub>O<sub>12</sub>-Mg<sub>3</sub>Al<sub>2</sub>Si<sub>3</sub>O<sub>12</sub>. *Physics Chemistry of Minerals* 27 (1), 3–10.
- Nakagawa, T., Buffett, B.A., 2005. Mass transport mechanism between the upper and lower mantle in numerical simulations of thermochemical mantle convection with multicomponent phase changes. *Earth Planet. Sci. Lett.* 230 (1), 11–27. <https://doi.org/10.1016/j.pepi.2004.10.007>.

- [org/10.1016/j.epsl.2004.11.005](https://doi.org/10.1016/j.epsl.2004.11.005).
- Nose, S., 1984. A molecular-dynamics method for simulations in the canonical ensemble. *Mol. Phys.* 52 (2), 255–268. <https://doi.org/10.1080/00268978400101201>.
- Oganov, A.R., Brodholt, J.P., Price, G.D., 2000. Comparative study of quasiharmonic lattice dynamics, molecular dynamics and Debye model applied to MgSiO<sub>3</sub> perovskite. *Phys. Earth Planet. Inter.* 122 (3–4), 277–288.
- Oganov, A.R., Brodholt, J.P., Price, G.D., 2001. The elastic constants of MgSiO<sub>3</sub> perovskite at pressures and temperatures of the Earth's mantle. *Nature* 411 (6840), 934–937. <https://doi.org/10.1038/35082048>.
- Pacalo, R.E.G., Weidner, D.J., 1997. Elasticity of majorite, MgSiO<sub>3</sub> tetragonal garnet. *Phys. Earth Planet. Inter.* 99 (1–2), 145–154.
- Pamato, M.G., Kurnosov, A., Ballaran, T.B., Frost, D.J., Ziberna, L., Giannini, M., ... Prakupenka, V.B., 2016. Single crystal elasticity of majoritic garnets: Stagnant slabs and thermal anomalies at the base of the transition zone. *Earth and Planetary Science Letters* 451, 114–124. <https://doi.org/10.1016/j.epsl.2016.07.019>.
- Panero, W.R., Stixrude, L., 2004. Hydrogen incorporation in stishovite at high pressure and symmetric hydrogen bonding in δ-AlOOH. *Earth Planet. Sci. Lett.* 221 (1–4), 421–431.
- Payne, M.C., Teter, M.P., Allan, D.C., Arias, T.A., Joannopoulos, J.D., 1992. Iterative minimization techniques for ab initio total-energy calculations: molecular dynamics and conjugate gradients. *Rev. Mod. Phys.* 64 (4), 1045.
- Perdew, J.P., Burke, K., Ernzerhof, M., 1996. Generalized gradient approximation made simple. *Phys. Rev. Lett.* 77 (18), 3865.
- Pigott, J.S., Wright, K., Gale, J.D., Panero, W.R., 2015. Calculation of the energetics of water incorporation in majorite garnet. *Am. Mineral.* 100 (5–6), 1065–1075. <https://doi.org/10.2138/am-2015-5063>.
- Rigden, S.M., Gwanmesia, G.D., Liebermann, R.C., 1994. Elastic-wave velocities of a pyrope majorite garnet to 3 GPa. *Phys. Earth Planet. Inter.* 86 (1–3), 35–44. [https://doi.org/10.1016/0031-9201\(94\)05060-0](https://doi.org/10.1016/0031-9201(94)05060-0).
- Ringwood, A., 1967. The pyroxene-garnet transformation in the earth's mantle. *Earth Planet. Sci. Lett.* 2 (3), 255–263.
- Ritsema, J., Xu, W., Stixrude, L., Lithgow-Bertelloni, C., 2009. Estimates of the transition zone temperature in a mechanically mixed upper mantle. *Earth Planet. Sci. Lett.* 277 (1–2), 244–252.
- Sato, Y., Akaogi, M., & Akimoto, S. (1978). Hydrostatic compression of synthetic garnets pyrope and almandine. *Journal of Geophysical Research*, 83(Nb1), 335–338. doi:<https://doi.org/10.1029/JB083iB01p00335>.
- Sawamoto, H., 1987. Phase diagram of MgSiO<sub>3</sub> at pressures up to 24 GPa and temperatures up to 2200 °C: phase stability and properties of tetragonal garnet. In *High Pressure Research in Mineral Physics: A Volume in Honor of Syun-iti Akimoto* 39, 209–219.
- Sinogeikin, S.V., Bass, J.D., 2000. Single-crystal elasticity of pyrope and MgO to 20 GPa by Brillouin scattering in the diamond cell. *Phys. Earth Planet. Inter.* 120 (1–2), 43–62. [https://doi.org/10.1016/S0031-9201\(00\)00143-6](https://doi.org/10.1016/S0031-9201(00)00143-6).
- Sinogeikin, S. V., & Bass, J. D. (2002a). Elasticity of majorite and a majorite-pyrope solid solution to high pressure: implications for the transition zone. *Geophysical Research Letters*, 29(2), 4–1–4. doi:<https://doi.org/10.1029/2001gl013937>.
- Sinogeikin, S.V., Bass, J.D., 2002b. Elasticity of pyrope and majorite-pyrope solid solutions to high temperatures. *Earth Planet. Sci. Lett.* 203 (1), 549–555. [https://doi.org/10.1016/S0012-821x\(02\)00851-8](https://doi.org/10.1016/S0012-821x(02)00851-8).
- Sinogeikin, S.V., Bass, J.D., O'Neill, B., Gasparik, T., 1997. Elasticity of tetragonal end-member majorite and solid solutions in the system Mg<sub>4</sub>Si<sub>4</sub>O<sub>12</sub>-Mg<sub>3</sub>Al<sub>2</sub>Si<sub>3</sub>O<sub>12</sub>. *Phys. Chem. Miner.* 24 (2), 115–121. <https://doi.org/10.1007/s002690050024>.
- Sinogeikin, S., Katsura, T., Bass, J.D., 1998. Sound velocities and elastic properties of Fe-bearing wadsleyite and ringwoodite. *Journal of Geophysical Research: Solid Earth* 103 (B9), 20819–20825.
- Sinogeikin, S.V., Bass, J.D., Katsura, T., 2001. Single-crystal elasticity of γ-(Mg<sub>0.91</sub>Fe<sub>0.09</sub>2SiO<sub>4</sub>) to high pressures and to high temperatures. *Geophys. Res. Lett.* 28 (22), 4335–4338.
- Stixrude, L., Lithgow-Bertelloni, C., 2005. Thermodynamics of mantle minerals - I. Physical properties. *Geophys. J. Int.* 162 (2), 610–632. <https://doi.org/10.1111/j.1365-246X.2005.02642.x>.
- Stixrude, L., Lithgow-Bertelloni, C., 2011. Thermodynamics of mantle minerals - II. Phase equilibria. *Geophys. J. Int.* 184 (3), 1180–1213. <https://doi.org/10.1111/j.1365-246X.2010.04890.x>.
- Stixrude, L., Lithgow-Bertelloni, C., 2012. Geophysics of chemical heterogeneity in the mantle. *Annual Review of Earth and Planetary Sciences*, Vol 40 (40), 569–595. <https://doi.org/10.1146/annurev.earth.36.031207.124244>.
- Thomson, A., Crichton, W., Brodholt, J., Wood, I., Siersch, N., Muir, J., ... Hunt, S., 2019. Seismic velocities of CaSiO<sub>3</sub> perovskite can explain LLSVPs in Earth's lower mantle. *Nature* 572 (7771), 643–647.
- Vinograd, V.L., Winkler, B., Putnis, A., Kroll, H., Milman, V., Gale, J.D., Fabrichnaya, O.B., 2006. Thermodynamics of pyrope-majorite, Mg<sub>3</sub>Al<sub>2</sub>Si<sub>3</sub>O<sub>12</sub>-Mg<sub>4</sub>Si<sub>4</sub>O<sub>12</sub>, solid solution from atomistic model calculations. *Mol. Simul.* 32 (2), 85–99. <https://doi.org/10.1080/08927020500501599>.
- Walker, A.M., Wookey, J., 2012. MSAT—a new toolkit for the analysis of elastic and seismic anisotropy. *Comput. Geosci.* 49, 81–90.
- Wallace, D.C., 1972. *Thermodynamics of Crystals*. Wiley, New York.
- Wallace, D., 1998. *Thermodynamics of Crystals*. Dover Publications, New York, pp. 484.
- Wang, Y., Grand, S.P., Tang, Y., 2014. Shear velocity structure and mineralogy of the transition zone beneath the East Pacific Rise. *Earth Planet. Sci. Lett.* 402, 313–323.
- Wang, Z.C., Ji, S.C., 2001. Elasticity of six polycrystalline silicate garnets at pressure up to 3.0 GPa. *Am. Mineral.* 86 (10), 1209–1218.
- Wang, Y.B., Weidner, D.J., Zhang, J.Z., Gwanmesia, G.D., Liebermann, R.C., 1998. Thermal equation of state of garnets along the pyrope-majorite join. *Phys. Earth Planet. Inter.* 105 (1–2), 59–71. [https://doi.org/10.1016/S0031-9201\(97\)00072-1](https://doi.org/10.1016/S0031-9201(97)00072-1).
- Weidner, D.J., Sawamoto, H., Sasaki, S., Kumazawa, M., 1984. Single-crystal elastic properties of the spinel phase of Mg<sub>2</sub>SiO<sub>4</sub>. *Journal of Geophysical Research: Solid Earth* 89 (B9), 7852–7860.
- Workman, R.K., Hart, S.R., 2005. Major and trace element composition of the depleted MORB mantle (DMM). *Earth Planet. Sci. Lett.* 231 (1–2), 53–72. <https://doi.org/10.1016/j.epsl.2004.12.005>.
- Xu, W., Lithgow-Bertelloni, C., Stixrude, L., Ritsema, J.J.E., Letters, P.S., 2008. The Effect of Bulk Composition and Temperature on Mantle Seismic Structure. 275(1–2). pp. 70–79.
- Yagi, T., Akaogi, M., Shimomura, O., Tamai, H., & Akimoto, S. (1987). High pressure and high temperature equations of state of majorite. *High-pressure Research in Mineral Physics*, edited by M. H. Manghni and Y. Syono, pp. 251–260, American Geophysical Union, Washington, D.C., 1987.
- Yagi, T., Uchiyama, Y., Akaogi, M., Ito, E., 1992. Isothermal compression curve of Mg<sub>3</sub>SiO<sub>3</sub> tetragonal garnet. *Phys. Earth Planet. Inter.* 74 (1–2), 1–7. [https://doi.org/10.1016/0031-9201\(92\)90063-2](https://doi.org/10.1016/0031-9201(92)90063-2).
- Yamazaki, D., Kato, T., Yurimoto, H., Ohtani, E., Toriumi, M., 2000. Silicon self-diffusion in MgSiO<sub>3</sub> perovskite at 25 GPa. *Physics of the Earth Planetary Interiors* 119 (3–4), 299–309.
- Yeganehhaeri, A., Weidner, D.J., Ito, E., 1990. Elastic properties of the pyrope-majorite solid-solution series. *Geophys. Res. Lett.* 17 (13), 2453–2456. <https://doi.org/10.1029/GL017i013p02453>.
- Yu, Y.G.G., Wentzcovitch, R.M., Vinograd, V.L., Angel, R.J., 2011. Thermodynamic properties of MgSiO<sub>3</sub> majorite and phase transitions near 660 km depth in MgSiO<sub>3</sub> and Mg<sub>2</sub>SiO<sub>4</sub>: a first principles study. *Journal of Geophysical Research-Solid Earth* 116, B02208. <https://doi.org/10.1029/2010jb007912>.
- Zhang, Z., Liu, Z., 2015. High pressure equation of state for molten CaCO<sub>3</sub> from first principles simulations. *Chin. J. Geochem.* 34 (1), 13–20.
- Zhang, L., Ahsbahs, H., Kutoglu, A., Geiger, C.A., 1999. Single-crystal hydrostatic compression of synthetic pyrope, almandine, spessartine, grossular and andradite garnets at high pressures. *Physics and Chemistry of Minerals* 27 (1), 52–58. <https://doi.org/10.1007/s002690050240>.
- Zhang, Z.G., Stixrude, L., Brodholt, J., 2013. Elastic properties of MgSiO<sub>3</sub>-perovskite under lower mantle conditions and the composition of the deep Earth. *Earth Planet. Sci. Lett.* 379, 1–12. <https://doi.org/10.1016/j.epsl.2013.07.034>.
- Zhang, Z.G., Mao, Z., Liu, X., Zhang, Y.G., Brodholt, J., 2018. Stability and reactions of CaCO<sub>3</sub> polymorphs in the Earth's deep mantle. *Journal of Geophysical Research-Solid Earth* 123 (8), 6491–6500. <https://doi.org/10.1029/2018jb015654>.
- Zou, Y.T., Irifune, T., Greaux, S., Whitaker, M.L., Shinmei, T., Ohfuji, H., ... Higo, Y., 2012. Elasticity and sound velocities of polycrystalline Mg<sub>3</sub>Al<sub>2</sub>(SiO<sub>4</sub>)<sub>3</sub> garnet up to 20 GPa and 1700 K. *Journal of Applied Physics* 112 (1), 014910. <https://doi.org/10.1063/1.4736407>.